Weak Kondo interaction in $Ce(M_xGa_{1-x})_4$ alloys, M = Ag and Au



1996 J. Phys.: Condens. Matter 8 2365

(http://iopscience.iop.org/0953-8984/8/14/011)

J. Phys.: Condens. Matter **8** (1996) 2365–2376. Printed in the UK

# Weak Kondo interaction in $Ce(M_xGa_{1-x})_4$ alloys, M = Ag and Au*

H Flandorfer†‖, P Rogl†, E Bauer‡, H Michor‡, R Hatzl‡, E Gratz‡ and C Godart§‖

† Institut für Physikalische Chemie der Universität Wien, A-1090 Wien, Währingerstraße 42, Austria

‡ Institut für Experimentalphysik der Technischen Universität Wien, A-1040 Wien, Wiedner Hauptstraße 8–10, Austria

§ CNRS—Laboratoire de Chimie Metallurgique des Terres Rares, Equipe de Recherche 209, Place Aristide Briand, F-92195 Meudon Cédex, France

‖ LURE, Université de Paris Sud, F-91405 Orsay, France

Received 10 October 1995

**Abstract.** The crystal structure of the title compounds has been characterized by quantitative room-temperature X-ray powder diffraction to be isotypic with the $BaAl_4$ type with partial disorder among the p-metal atoms. The low-temperature behaviour of these alloys is characterized by a decrease of the ordering temperatures as the Au content increases. Weak Kondo interaction for alloys richest in Au is observed from various transport and specific heat measurements.

## 1. Introduction

Extended solution ranges have been reported recently for the alloy series $Ce(M_xGa_{1-x})_4$, M = Cu, Ag, Au [1–3]. These compounds were found to adopt either the $BaAl_4$-type or the derivative $CaBe_2Ge_2$-type structure [1–3]. At high temperatures, these ternary compounds are characterized by an effective magnetic moment of roughly 2.6 $\mu_B$, in agreement with a trivalent ground state of cerium. Magnetic ordering exists below 3 K and the ordering temperature decreases when the gallium content decreases. The most prominent member of this family of compounds with an ordered $BaAl_4$ type appears to be $CeCu_2Si_2$ [4]. A variety of interesting physical phenomena have already been found from investigations of cerium-containing systems with the $BaAl_4$ type such as $CeCuAl_3$, $Ce(Ga_{1-x}Ni_x)_4$ [6, 7] and $Ce(Cu_xGa_{1-x})_4$ [7]. The ground state properties of these compounds exhibiting a tetragonal crystal structure depend sensitively on (i) crystal field splitting, (ii) the mutual interaction of the Kondo effect—tending to screen the cerium moments—and (iii) the RKKY interaction—responsible for long-range magnetic order. In the present paper we give an overview of the low-temperature behaviour of the alloy series $Ce(M_xGa_{1-x})_4$, M = Cu, Ag, Au, concerning direct measurements of the cerium valence by XAS (X-ray absorption spectroscopy) as well as measurements of the specific heat and the field and temperature dependent electrical resistivity. Since the physical properties of these compounds are essentially determined by the distribution of atoms in the crystal, the crystal structures of the compounds $Ce(Ag_{0.16}Ga_{0.84})_4$ and $Ce(Au_xGa_{1-x})_4$ for $x = 0.1$, 0.15 and 0.25 have been established by X-ray powder techniques.

* dedicated to Professor R Ferro on the occasion of his 70th birthday.

0953-8984/96/142365+12$19.50  

## 2. Experimental details

All samples, each of about 2 g, were synthesized by repeated arc melting the high-purity elements together in a titanium-gettered argon atmosphere starting from the nominal composition RE:(M, Ga) = 1:4. Weight losses due to the arc melting process were checked to be less than 0.5 mass%. The types and impurity levels of the starting materials are as follows: RE(Ce, La), ingot, m3N, Auer-Remy, Germany; Cu, rod m3N, Alpha Ventron, Germany; Ag, powder, puriss., Ögussa, Austria; Au, shot, 3N, Ögussa, Austria; Ga, m4N, Alcan Electronics, CH. After melting the reguli were packed in molybdenum foil, sealed in evacuated silica tubes and heat treated for 340 h at 600 °C in a wire-wound power controlled tubular furnace calibrated against a Pt/PtRh thermocouple. After annealing the samples were quenched by casting the silica tubes into cold water.

Precise lattice parameters and standard deviations were obtained by a least-squares refinement of room-temperature Guinier–Huber X-ray (Cu K$\alpha_1$) powder data employing an internal standard of 99.9999 mass% pure Ge ($a_{Ge} = 0.565\,790\,6$ nm). For quantitative refinement of the atom positions, the X-ray intensities were recorded from a flat specimen in a Siemens D5000 automatic powder diffractometer (Cu K$_\alpha$). Full-matrix full-profile Rietveld refinements were performed employing a PC version of the program by Wiles and Young [8]. X-ray absorption measurements were performed at the French synchrotron radiation facility of LURE using the X-ray beam delivered by the DCI storage ring, working at 1.85 GeV–∼320 mA, on the EXAFS 2 station. A double Si(311) crystal was used as a monochromator. Rejection of harmonics of order three was achieved by two parallel mirrors adjusted to cut off energies higher than ∼9 keV in the incident beam. Experiments were made in the range (5660–5840 eV around the $L_{III}$ edge of Ce. Powdered samples were spread on adhesive Kapton tape and three such tapes were stacked out to make a sufficiently thick sample to provide the expected amplitude of the discontinuity as well as to avoid any holes in the powder distribution. Samples were also measured in a cryostat kept at a constant temperature of ∼10 K. No runs versus temperature were performed to avoid loss in beam time. After subtracting the background from the spectra in a standard manner, $L_{III}$ edge deconvolutions were made using a technique already described in [9] and [10]. Resistivity data were taken from bar shaped samples, using a four-probe d.c. method. Fields up to 10 T were generated by a superconducting magnet. A differential method with lead as reference material was used to obtain temperature-dependent thermopower data. Specific heat measurements up to 9 T were carried out on 1–2 g samples in two automated calorimeters (1.5–100 K) using a quasi-adiabatic step heating technique. The temperature was measured either with a germanium resistor or with a carbon glass resistor for zero-field or field measurements, respectively; these were situated in the bore of the sapphire sample holder. The field calibration of the latter was performed *in situ* against an $SrTiO_3$ sensor.

## 3. Results and discussion

Our results of the X-ray characterization in comparison with the lattice parameter data reported earlier [1–3] are presented in table 1. For all compounds investigated the determined lattice parameters are in good agreement with the literature data.

### *3.1. X-ray characterization and refinement of the crystal structure of Ce($Ag_{0.16}Ga_{0.84}$)$_4$*

The room-temperature X-ray powder diffractogram of $Ce(Ag_{0.64}Ga_{3.36})_4$ was evaluated by a full-matrix full-profile Rietveld refinement. The results are summarized in table 2 and

**Table 1.** Crystallographic data for the ternary solid solutions Ce{(Ag, Au)$_x$Ga$_{1-x}$}$_4$.

| Phase Comp. in at.% | Phase Analys. | Space Group | Sruct. Type | Unit Cell Dimensions in nm | | | | Ref. |
|---|---|---|---|---|---|---|---|---|
| | | | | a | c | V | c/a | |
| $Ce_{20}Ag_{13}Ga_{67}$ | $CeAg_{0.65}Ga_{3.35}$ | I4/mmm | $BaAl_4$ | 0.4313(2) | 1.0745(6) | 0.1999 | 2.4913 | |
| | | | | 0.4318(2) | 1.0737(3) | 0.2002 | 2.4866 | [2] |
| $Ce_{20}Au_8Ga_{72}$ | $CeAu_{0.4}Ga_{3.6}$* | I4/mmm | $BaAl_4$ | 0.4357(1) | 1.0172(3) | 0.1931 | 2.3346 | |
| $Ce_{20}Au_8Ga_{72}$ | $CeAu_{0.4}Ga_{3.6}$* | I4/mmm | $BaAl_4$ | 0.4356(1) | 1.0248(2) | 0.1945 | 2.3525 | |
| $Ce_{20}Au_{12}Ga_{68}$ | $CeAu_{0.6}Ga_{3.4}$* | I4/mmm | $BaAl_4$ | 0.4354(1) | 1.0582(7) | 0.2006 | 2.4302 | |
| | | | | 0.4353(2) | 1.0586(9) | 0.2006 | 2.432 | [3] |
| $Ce_{20}Au_{16}Ga_{64}$ | $CeAu_{0.8}Ga_{3.2}$ | I4/mmm | $BaAl_4$ | 0.4345(1) | 1.0644(4) | 0.2009 | 2.4495 | |
| $Ce_{20}Au_{20}Ga_{60}$ | $CeAuGa_3$* | I4/mmm | $BaAl_4$ | 0.4339(1) | 1.0672(4) | 0.2010 | 2.4594 | |
| | | | | 0.4340(2) | 1.0663(4) | 0.2008 | 2.457 | [3] |
| $Ce_{20}Au_{22}Ga_{58}$ | $CeAu_{1.1}Ga_{2.9}$* | I4/mmm | $BaAl_4$ | 0.4338(1) | 1.0674(5) | 0.2012 | 2.4606 | |
| | | | | 0.4337(1) | 1.0677(4) | 0.2008 | 2.4621 | |
| | | | | 0.4335(2) | 1.0699(3) | 0.2010 | 2.468 | [3] |
| $Ce_{20}Au_{24}Ga_{56}$ | $CeAu_{1.2}Ga_{2.8}$ | I4/mmm | $BaAl_4$ | 0.4337(1) | 1.0672(2) | 0.2007 | 2.4608 | |
| $Ce_{20}Au_{30}Ga_{50}$ | $CeAu_{1.5}Ga_{3.5}$ | P4/nmm | $CaBe_2Ge_2$ | 0.4349(1) | 1.0636(4) | 0.2012 | 2.4456 | |
| | | | | 0.4356(1) | 1.0631(7) | 0.2017 | 2.4404 | |
| | | | | 0.4349(2) | 1.0671(6) | 0.2019 | 2.454 | [3] |
| $La_{20}Au_{22}Ga_{58}$ | $LaAu_{1.1}Ga_{2.9}$* | I4/mmm | $BaAl_4$ | 0.4370(1) | 1.0664(2) | 0.2036 | 2.4403 | |
| $La_{20}Au_{30}Ga_{50}$ | $LaAu_{1.5}Ga_{2.5}$ | P4/nmm | $CaBe_2Ge_2$ | 0.4388(1) | 1.0604(4) | 0.2041 | 2.4166 | |
| | | | | 0.4379(1) | 1.0632(7) | 0.2039 | 2.4280 | [3] |

*Sample contains small amounts of $Ce_2O_3$;

confirm the crystal symmetry consistent with the $BaAl_4$ type. Ce occupies the 2a sites. The free atomic parameter of the 4e site was refined to $z = 0.3844(2)$; the reliability factor obtained was $R_I = 0.066$ (see also table 2). Silver and gallium atoms are distributed over the 4d and 4e sites, but silver atoms show a distinct preference for the 4d site, i.e. 75% of the silver atoms are found in 4d. This is in contrast to the results of a structure determination of isotypic $Pr(Ag_{0.18}Ga_{0.82})_4$ [1]. There the 4d site is occupied only by gallium atoms and silver is found in the 4e site.

### *3.2. X-ray characterization and refinement of the crystal structure of Ce($Au_xGa_{1-x}$)$_4$, $x = 0.1$, 0.15, and 0.25*

Full-profile Rietveld refinements of alloys $Ce(Ag_xGa_{1-x})_4$ revealed the substitution mode along the series with increasing gold concentration. At low levels of gold Au atoms preferentially occupy the 4e dumbbell sites with interatomic distances as short as 0.260 nm suggesting rather tight binding. Reaching a maximum level of about 50% gold in the 4e sites, the excess gold is found to gradually enter the 4d sites. For the details of the refinement see table 3.

A comparison of the observed and calculated X-ray powder profiles is shown in figure 1 for one of the alloys, $Ce(Au_{0.25}Ga_{0.75})_4$.

### *3.3. X-ray absorption spectroscopy*

In agreement with the results of the magnetic measurements in [1–3], the determination of the cerium valence with XAS (X-ray absorption spectroscopy) at ∼10 K and RT reveals a trivalent state of cerium for all compounds investigated. The spectra shown in figures 2 and 3 indicate the absence of any significant contribution associated with a $Ce^{4+}$ state to be expected at 5732 eV.

**Table 2.** Crystallographic data of $Ce(Ag_{0.16}Ga_{0.84})_4$, quenched from 500 °C.

| | | | | | | | |
|---|---|---|---|---|---|---|---|
| Method | Full profile refinement of room temperature X-ray powder diffraction data<br>Number of reflections used in refinement : 42, $20° \le 2\theta \le 100°$ | | | | | | |
| Lattice param.* | a = 0.4313(2) nm, c = 1.0745(6) nm, V = 0.1999 $nm^3$, c/a = 2.491 | | | | | | |
| Structure type | $BaAl_4$ | | | | | | |
| Space group | I4/mmm - $D_{4h}^{17}$, No. 139, origin at $\bar{1}$, Z = 2 | | | | | | |
| Residual values | $R_I = 0.066$, $R_F = 0.079$, $R_P = 0.099$, $R_{wP} = 0.105$ | | | | | | |
| Atom parameter | *Atom* | *Site* | *x* | *y* | *z* | *B in* $10^{-2}$ $nm^2$ | *Occupation* |
| | Ce | 2a | 0 | 0 | 0 | 0.1 | 1 |
| | $(Ag,Ga)_1$ | 4d | 0 | 0.5 | 0.25 | 0.60(9) | 24% Ag+76% Ga |
| | $(Ag,Ga)_2$ | 4e | 0 | 0 | 0.3844(2) | 0.30(7) | 8% Ag+92% Ga |
| Pref. Orient. Parameter | -0.027(5) along [001] | | | | | | |
| Interatomic dist. (in nm) | *Central Atom: Ce* | | *Central Atom:* $(Ag,Ga)_1$ | | *Central Atom:* $(Ag,Ga)_2$ | | |
| | *Ligand Atom* | *Distance* | *Ligand Atom* | *Distance* | *Ligand Atom* | *Distance* | |
| | 4 Ce | 0.4315 | 4 Ce | 0.3443 | 1 Ce | 0.4120 | |
| | 2 $(Ag,Ga)_2$ | 0.4120 | 4 $(Ag,Ga)_1$ | 0.3051 | 4 Ce | 0.3296 | |
| | 8 $(Ag,Ga)_1$ | 0.3443 | 4 $(Ag,Ga)_2$ | 0.2592 | 4 $(Ag,Ga)_1$ | 0.2592 | |
| | 8 $(Ag,Ga)_2$ | 0.3296 | | | 1 $(Ag,Ga)_2$ | 0.2495 | |

*Lattice parameters determined from Guinier film

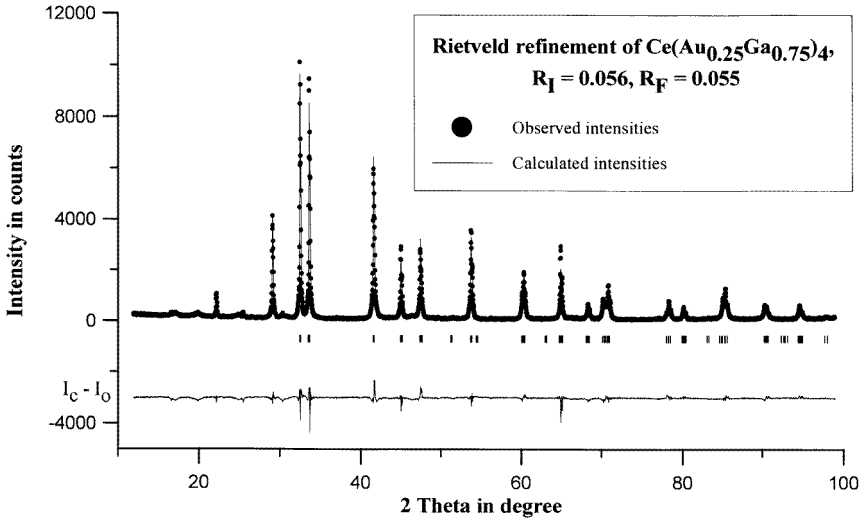


**Figure 1.** A graphic presentation of the full-profile Rietveld refinement of $Ce(Au_{0.25}Ga_{0.75})_4$.

### *3.4. Transport properties*

Figure 4 shows the temperature dependence of the electrical resistivity $\rho$ for several alloys of $CeAu_xGa_{4-x}$ in a normalized representation. Due to the brittleness of the samples, the absolute resistivity varies and therefore no continuous concentration-dependent behaviour, even in the normalized plot, can be distinguished. The inset of figure 4 shows the low-

**Table 3.** Crystallographic data of $Ce(Au_xGa_{1-x})_4$ samples, quenched from 600 °C.

| Method | Full profile Rietveld refinement of X-ray powder diffraction | | |
|---|---|---|---|
| Space group | I 4/mmm - $D_{4h}^{17}$, No. 139, origin at $\bar{1}$, Z = 2 | | |
| Structure type | $BaAl_4$ | | |
| Compound | $Ce_{20}Au_8Ga_{72}$ | $Ce_{20}Au_{12}Ga_{68}$ | $Ce_{20}Au_{20}Ga_{60}$ |
| No. of reflections used | 39 | 40 | 46 |
| 2θ range | 25° - 100° | 25° - 100° | 10° - 100° |
| *Lattice parameters*[1]*:* | | | |
| a | 0.4356(1) nm | 0.4354(1) nm | 0.4339(1) nm |
| c | 1.0248(2) | 1.0582(7) nm | 1.0672(4) nm |
| V | 0.1945 | 0.2006 $nm^3$ | 0.2010 $nm^3$ |
| c/a | 2.3525 | 2.4302 | 2.4594 |
| *Residual values:* | | | |
| $R_I$ | 0.081 | 0.066 | 0.056 |
| $R_F$ | 0.072 | 0.036 | 0.055 |
| $R_P$ | 0.221 | 0.162 | 0.096 |
| $R_{wP}$ | 0.284 | 0.202 | 0.125 |
| *Atomic parameters* | | | |
| 2a site (0 0 0) | | | |
| Temperature parameter B | 1.5(2) | 0.3(1) $10^{-2}nm^2$ | 0.41(5) $10^{-2}nm^2$ |
| Occupation | Ce | Ce | Ce |
| 4d site (0 0.5 0.25) | | | |
| Temperature parameter B | 2.0(2) | 0.4(1) $10^{-2}nm^2$ | 0.77(6) $10^{-2}nm^2$ |
| Occupation | Ga | Ga | 8 % Au + 92 % Ga |
| 4e site (0 0 z) | | | |
| z | 0.3806(5) | 0.3814(2) | 0.3787(1) |
| Temperature parameter B | 1,5(2) | 0.20(9) $10^{-2}nm^2$ | 0.17(4) $10^{-2}nm^2$ |
| Occupation | 20 % Au + 80 % Ga | 30 % Au + 70 % Ga | 49 % Au + 51 % Ga |
| *Interatomic distances:* | | | |
| Ce - 4 Ce | 0.4356 | 0.4354 | 0.4339 |
| Ce - 2 $(Au,Ga)_{4e}$ | 0.3901 | 0.4036 | 0.4042 |
| Ce - 8 $(Au,Ga)_{4d}$ | 0.3363 | 0.3426 | 0.3439 |
| Ce - 8 $(Au,Ga)_{4e}$ | 0.3314 | 0.3325 | 0.3330 |
| $(Au,Ga)_{4d}$ - 4 Ce | 0.3363 | 0.3426 | 0.3439 |
| $(Au,Ga)_{4d}$ - 4 $(Au,Ga)_{4d}$ | 0.3080 | 0.3079 | 0.3068 |
| $(Au,Ga)_{4d}$ - 4 $(Au,Ga)_{4e}$ | 0.2556 | 0.2583 | 0.2568 |
| $(Au,Ga)_{4e}$ - 1 Ce | 0.3901 | 0.4036 | 0.4042 |
| $(Au,Ga)_{4e}$ - 4 Ce | 0.3314 | 0.3325 | 0.3330 |
| $(Au,Ga)_{4e}$ - 4,[1][2] $(Au,Ga)_{4e}$ | 0.2556 | 0.2583 | 0.2589 |
| $(Au,Ga)_{4e}$ - 1,[4][2] $(Au,Ga)_{4e}$ | 0.2447 | 0.2510 | 0.2568 |

[1]Lattice parameters determined from Guinier film
[2]Values in square brackets are valid for $Ce_{20}Au_{20}Ga_{60}$

temperature resistivity (again in a normalized representation) for various $Ce(Au, Ga)_4$ alloys. Obvious from this plot is the onset of long-range magnetic order in the Ga-rich compounds as observed from that temperature below which $\rho(T)$ starts to decrease markedly. In contrast, no sign of long-range magnetic order is visible in the Au-rich compounds down to about 1.4 K. However, these alloys exhibit shallow minima around 10 K. Such a behaviour is usually attributed to a Kondo-type interaction present in Ce-based compounds. At somewhat

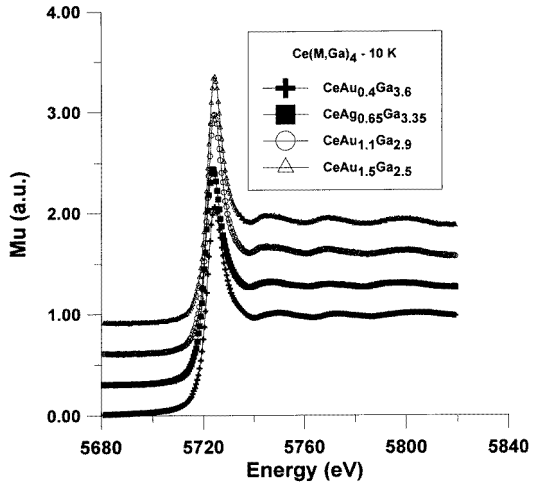


**Figure 2.** X-ray absorption spectra of selected samples at ∼10 K.

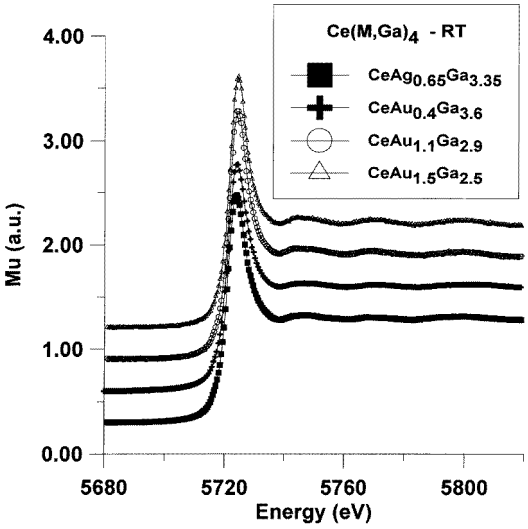


**Figure 3.** X-ray absorption spectra of selected samples at ∼290 K.

elevated temperatures (about 50–100 K) the negative curvature of $\rho(T)$ reflects, most probably, crystal field splitting of the sixfold degenerate ground state in these tetragonal compounds.

The presence of weak Kondo interaction in the Au-rich alloy is also reflected from measurements of the magnetoresistance, shown for $CeAu_{1.5}Ga_{2.5}$ in figure 5 for different temperatures. The field-dependent behaviour of $\rho(B)/\rho(0)$, (here, $\rho(B)$ and $\rho(0)$ are the resistivities with and without external field, respectively) is characterized by a continuous decrease with increasing external fields. Besides minima in the temperature dependent resistivity, the monotonic decrease of $\rho(B)/\rho(0)$ with rising fields can be taken as a 'fingerprint' of Kondo interaction. Considering Kondo scattering processes at $T = 0$, $\rho(B)/\rho(0)$ has been calculated by Schlottmann [11] for various values of the total angular

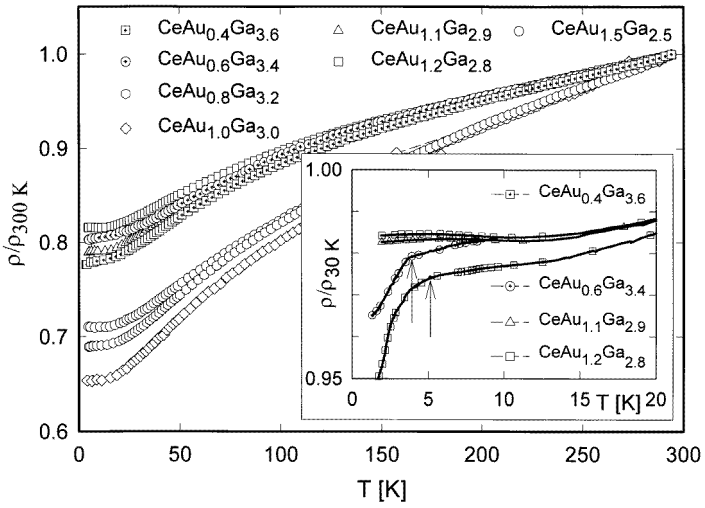


**Figure 4.** The temperature-dependent resistivity $\rho$ of various Ce(Au, Ga)$_4$ alloys in a normalized representation. The inset shows the low-temperature behaviour in more detail.

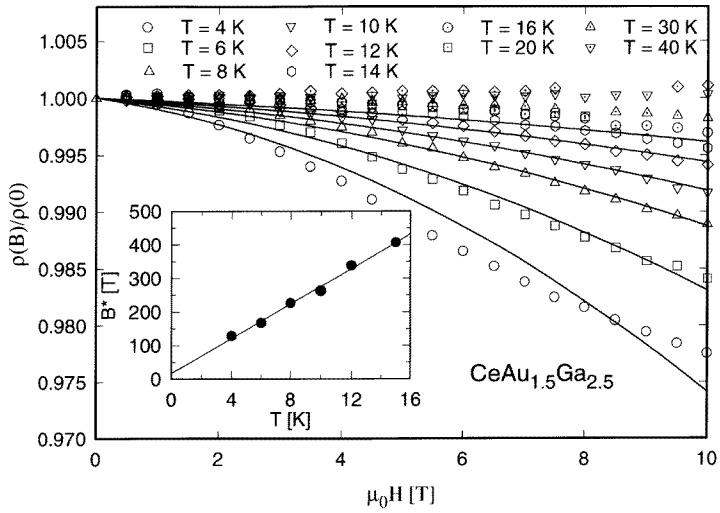


**Figure 5.** The field-dependent magnetoresistance $\rho(B)/\rho(0)$ of $CeAu_{1.5}Ga_{2.5}$ for different temperatures. The solid lines are least-squares fits explained in the text. The inset shows the characteristic field $B^*$ as a function of temperature. The solid line is a least-squares fit according to equation (1).

momentum. He demonstrated that the field dependence of $\rho(B)/\rho(0)$ is determined by a single parameter, the characteristic field $B^*$. For finite temperatures, an approximation has been given in [12] and [13], indicating that $B^*$ increases linearly with temperature, i.e.

$$B^*(T) = B^*(0) + k_B T/g\mu \tag{1}$$

where $g$ and $\mu$ are the Landé factor and the magnetic moment of the Kondo ion. $B^*(0)$ has the meaning of the Kondo field and is related to the single-ion Kondo temperature via

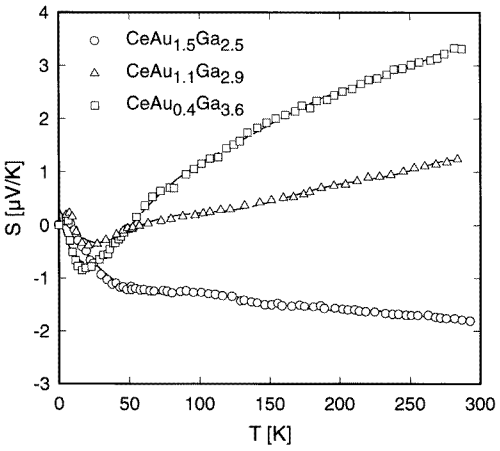


**Figure 6.** The temperature dependent thermopower of various $Ce(Au, Ga)_4$ alloys.

$T_K = B^*(0)g\mu/k_B$. The field $B^*(0)$ is sufficient to suppress the Kondo resonance near the Fermi energy. The experimental data have been fitted taking into account the theoretical field—and the approximated temperature dependence of the magnetoresistance of Kondo systems (solid lines, figure 5). Discrepancies obvious between the data and the theoretical dependence are thought to originate from the classical magnetoresistance, which usually yields a positive contribution, whilst it is not incorporated in the calculation. Moreover, the cited theoretical model calculation considers just the interaction of electrons with the Ce moments, while for a real crystal additional interactions are present. Unfortunately, no reliable procedure is available to separate the total measured magnetoresistance into its individual contributions.

Neglecting these uncertainties, we have determined whether $\rho(B)/\rho(0)$ obeys equation (1), by plotting the characteristic fields $B^*(T)$ as a function of temperature (inset, figure 5). A linear extrapolation of the data towards zero temperature yields $B^*(0) = 17$ T; together with the slope of this linear extrapolation, a Kondo temperature of the order of 1 K can be evaluated.

In figure 6, the temperature-dependent thermopower $S(T)$ is displayed for $x = 0.4$, 1.1 and 1.5. It is interesting to note that at higher temperatures there is a crossover from positive thermopower values for Ga-rich alloys to a negative thermopower for the Au-rich alloys of this series. The behaviour of $S(T)$ of $CeAu_{1.5}Ga_{2.5}$ resembles that of the isostructural magnetically ordered Kondo compound $CeCuAl_3$ [5]. The absolute values observed for this series are smaller than those measured for archetypal systems such as $CeCu_2$ or $CeCu_6$. It is thought that due to the weak Kondo interaction, i.e. a small value of $T_K$, the Kondo contribution to $S(T)$ does not very much influence the observed data. This is due to the fact that the different contributions to the total measured effect are just added together in a weighted manner according to the Nordheim–Gorter rule.

### *3.5. Specific heat*

Figure 7 shows the temperature dependence of the specific heat $c$ for various compounds of $Ce(Au_xGa_{1-x})_4$ and for $CeAg_{0.65}Ga_{3.35}$. These measurements clearly indicate that long-range magnetic order is weakened according to the lowering of Ga content. For compounds

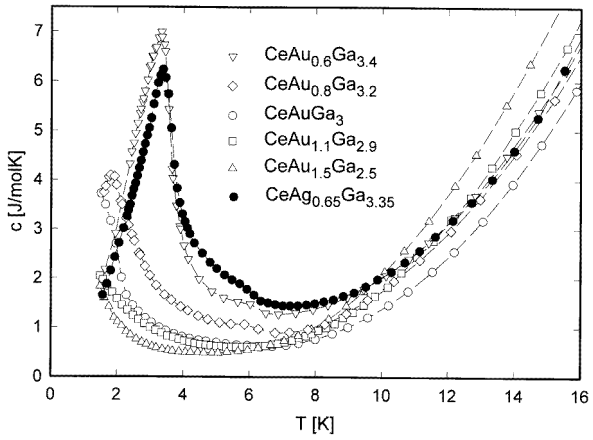


**Figure 7.** The temperature-dependent specific heat $c$ for different Ce(Au, Ga)$_4$ alloys and for $CeAg_{0.65}Ga_{3.35}$.

with Ga concentrations $x \leqslant 0.25$, long-range order is suppressed below 1.5 K. The ordering temperatures themselves are found to be slightly below those reported in [3]. Furthermore, the ordering temperature of the Ag-based alloy does not differ very much from that of the compound with a similar Au content. This proves that either the Au or the Ag substitution of Ga yields a similar magnetic state in these series of alloys. However, very frequently Au and Ag substitutions in a particular compound can originate drastic differences in the respective ground states [14, 15].

It is interesting to note that the jump in the specific heat $\delta c_{mag}$ at $T = T_{mag}$ appears to be reduced with respect to the expected value for a ground state doublet. Within the mean-field theory $\delta c_{mag}$ of the latter is equal to 12.5 J mol$^{-1}$ K$^{-1}$ [16]. Moreover, the magnetic entropy associated with the phase transition at $T = T_{mag}$ does not release the full entropy of $R \ln 2$. Different factors can account for this observation. First of all, short-range order effects may cause a broad tail of the heat capacity above the ordering temperature. Next, sample inhomogeneities yield usually to a much broader transition than that calculated within the mean-field theory. In the light of the presented transport measurements, Kondo-type interactions may also be responsible for the reduced value of $\delta c_{mag}$.

A competition between the Kondo effect $k_B T_K$ and RKKY (Rundermann–Kittel–Kasuya–Yoshida) interaction can result in long-range magnetic order, however, with reduced magnetic moments. Consequently the jump in the specific heat at $T = T_{mag}$ is much lower than the expected value of 12.5 J mol$^{-1}$ K$^{-1}$ and additional entropy is spread over a considerable broad temperature range. Such a behaviour can be accounted for on the basis of a phenomenological model [17], which has been successfully applied to moment-reduced systems such as $CeCu_5$ [18]. This model is based on the Kondo effect, represented in the scope of calculations of Schotte and Schotte [19], and incorporates magnetic order within a mean-field approximation. Applying this model to the experimental data allows us to extract the Kondo temperature $T_K$ and the mean-field constant $\Im$. To establish whether this phenomenological model is able to account for the experimental data, we have tried to adjust the mean-field constant $\Im$ and the Kondo temperature $T_K$ so as to describe the data in a reasonable manner.

Figure 8 shows the magnetic contribution to the specific heat, $c_{mag}$, of Ce($Au_xGa_{1-x}$)$_4$, $x = 0.20$ and 0.15. For the former compound, additional measurements at external fields

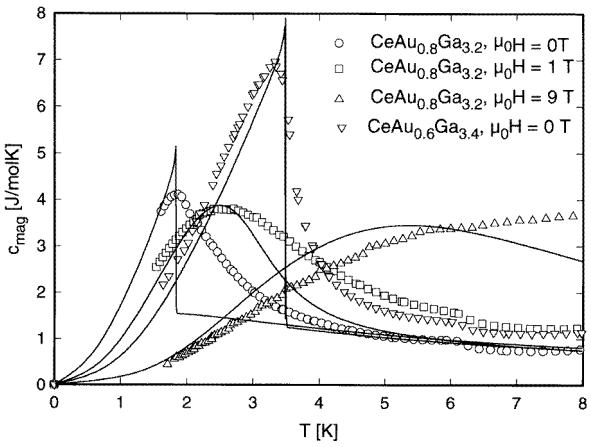


**Figure 8.** The temperature-dependent magnetic contribution to the specific heat $c_{mag}$ of $Ce(Au_xGa_{1-x})_4$, $x = 0.2$, 0.15, at different values of magnetic fields. The solid lines are fits according to the phenomenological model described in the text.

of 1 T and 9 T have been performed. $c_{mag}(T)$ has been evaluated from the experiment by subtracting the $c_P$ of the appropriate La compound. These data indicate a rather broad phase transition which becomes completely smeared out at a field of 9 T. The solid lines in figure 8 represent the fit of the mentioned model to the data where the following parameters have been evaluated: $\Im = 10.5$ K, $T_K = 3$ K for $CeAu_{0.6}Ga_{3.4}$ and $\Im = 7.7$ K, $T_K = 3.3$ K for $CeAu_{0.8}Ga_{3.2}$. The latter values, of course, have been applied also in the case of finite magnetic fields. Beside some disadvantages of this model, such as the fact that no broadened phase transitions or short-range order effects above $T_{mag}$ can be accounted for, some archetypal hints for the simultaneous presence of the Kondo effect and long-range magnetic order are correctly displayed. For example, the reduced jump of $c_{mag}$ at $T_{mag}$ and the nonvanishing contribution in the paramagnetic temperature range due to the Kondo effect are shown. The field dependence of $c_{mag}(T)$ and the theoretical description indicate a ferromagnetic ground state, in accordance with previously reported magnetization measurements [3].

Based on this model, it is possible to estimate the moment reduction owing to the Kondo effect, when compared to the unperturbed values of the respective crystal field ground states. For $x = 0.15$ and $x = 0.2$ reductions of 22% and 39% have been evaluated. These values, however, should be considered as an upper boundary since short-range order effects and the broad transition are not incorporated in this calculation. Moreover these effects cause an overestimation of $T_K$.

In figure 9, $c_{mag}(T)$ of $CeAg_{0.65}Ga_{3.35}$ is plotted for temperatures up to 40 K. In addition to the contributions of long-range magnetic order and the Kondo effect, a Schottky contribution due to crystal field splitting is obvious. Applying again the cited model reveals $\Im = 12$ K and $T_K = 5$ K (long-dashed line, figure 9). Both values together lead to a reduction of about 35% of the magnetic moments compared to the case without a Kondo effect. Again, this value is an upper border for reasons mentioned above. The short-dashed line at elevated temperatures is a least-squares fit according to the Schottky contribution giving a preliminary level scheme of about 0–65–700 K. However, the value of the uppermost level does not influence sensitively the Schottky contribution in the investigated temperature range. The magnetic entropy associated with the phase transition at about 3.5 K

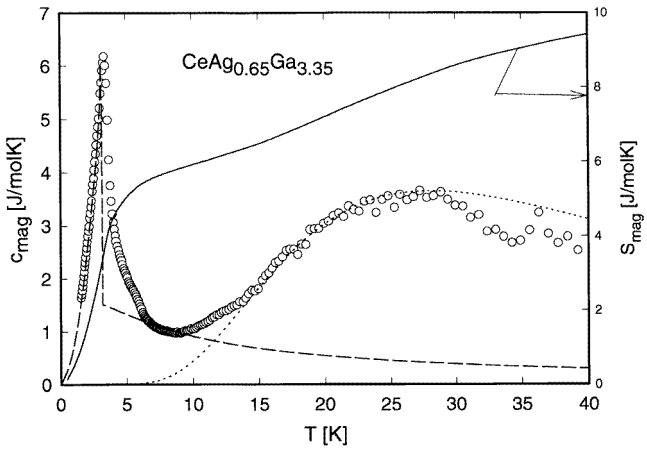


**Figure 9.** The temperature-dependent magnetic contribution to the specific heat $c_{mag}$ of $CeAg_{0.65}Ga_{3.35}$. The long-dashed line is a fit according to the phenomenological model described in the text; the short-dashed line represents the Schottky contribution with a level scheme 0–65–700 K. The solid line shows the magnetic entropy $S_{mag}(T)$.

(solid line) does not attain the theoretical value of $R \cdot \ln 2$ (5.76 J mol$^{-1}$ K$^{-1}$), which is recovered in the vicinity of 10 K.

## 4. Summary

The title compounds have been synthesized by arc melting followed by heat treatment at 600 °C. The crystal structures of $Ce(Ag_{0.16}Ga_{0.84})_4$ and $Ce(Au_xGa_{1-x})_4$ for $x = 0.1$, 0.15 and 0.25 have been refined from room-temperature X-ray powder data employing the Rietveld full-matrix full-profile method ($BaAl_4$ type; $R_I = 0.066$, 0.081, 0.066, 0.056, respectively). Whereas silver atoms were observed to show distinct preference for the 4d sites (0.24 Ag + 0.76 Ga), gold atoms at low gold concentration favour the 4e sites up to about 50% occupation before entering the 4d sites. Investigations of low-temperature physical properties indicated that the substitution of gallium by gold in $Ce(Au_xGa_{1-x})_4$ causes a decrease of the onset temperature of long-range magnetic order. However, even for the compounds richest in gold, i.e. $CeAu_{15}Ga_{2.5}$, an indication of long-range magnetic order well below 1.5 K can be seen from the rapid rise of $c(T)$ below the 2 K. If the appropriate data are analysed in the scope of models based on the Kondo effect, a rather low Kondo temperature $T_K$ is evaluated. Thus, RKKY interaction dominates and long-range magnetic order seems to prevail in the whole concentration range.

## Acknowledgment

This research has been supported by the Austrian National Science Foundation (FFWF) under grants P8218 and P10269.

## References

[1] Grin Yu N, Hiebl K, Rogl P and Noël H 1990 *J. Less Common Met.* **162** 371

[2] Grin Yu N, Hiebl K, Rogl P and Eibler R 1986 *J. Less Common Met.* **115** 367
[3] Grin Yu N, Rogl P, Wagner F E and Noël H 1987 *J. Solid State Chem.* **70** 168
[4] Steglich F, Aarts J, Bredl C D, Lieke W, Meschede D, Franz W and Schäfer J 1979 *Phys. Rev. Lett.* **43** 1892
[5] Bauer E, Pillmayr N, Gratz E, Hilscher G, Gignoux D and Schmitt D 1987 *Z. Phys.* B **67** 205
[6] Sampathkumaran E V, Hirota K, Das I and Tshikawa M 1993 *Phys. Rev.* B **47** 8349
[7] Sampathkumaran E V and Das I 1992 *Solid State Commun.* **81** 901
[8] Wiles D B and Young R A 1981 *J. Appl. Crystallogr.* **14** 151 (LNS/ILL-Version, J Rodriguez)
[9] Röhler J 1985 *J. Magn. Magn. Mater.* **47 & 48** 175
[10] Bonnin D, Kaiser P, Desbarres J and Fretigny C 1988 *Ecole CNRS 'Structure Fines d'Absorption des Rayons X' (Garchy)*
[11] Schlottmann P 1989 *Z. Phys.* B **51** 233
[12] Kawakami N and Okiji A 1986 *J. Phys. Soc. Japan* **55** 2114
[13] Batlogg B, Bishop D J, Bucher E, Golding B, Ramirez A P, Fisk Z, Smith J L and Ott H R 1987 *J. Magn. Magn. Mater.* **63 & 64** 441
[14] Bauer E, Gratz E, Hauser R, Le Tuan, Galatanu E, Kottar A, Michor H, Perthold W, Hilscher G, Kagayama T, Oomi G, Ichimiya N and Endo S 1994 *Phys. Rev.* B **50** 9300
[15] Bauer E, Hauser R, Gratz E, Payer K, Oomi G and Kagayama T 1993 *Phys. Rev.* B **48** 15 873
[16] Besnus M J, Braghta A, Hamdoui N and Meyer A 1992 *J. Magn. Magn. Mater.* **104 & 107** 1385
[17] Braghta A 1989 *PhD Thesis* University of Strasbourg
[18] Bauer E, Rotter M, Keller L, Fischer P, Ellerby M and McEwen K A 1994 *J. Phys.: Condens. Matter* **6** 5533
[19] Schotte K D and Schotte U 1975 *Phys. Lett.* **55A** 38